ChemPubSoc Europe

DOI: 10.1002/celc.201801280

CHEMELECTROCHEM Communications

Bismuth Oxychloride Nanoplatelets by Breakdown Anodization

Hanna Sopha,*[a, b] Zdenek Spotz,[b] Jan Michalicka,[b] Ludek Hromadko,[a] Roman Bulanek,[c] Tomas Wagner,[d] and Jan M. Macak*[a, b]

Herein, the synthesis of BiOCl nanoplatelets of various dimensions is demonstrated. These materials were prepared by anodic oxidation of Bi ingots in diluted HCl under dielectric breakdown conditions, triggered by a sufficiently high anodic field. Additionally, it is shown that the use of several other common diluted acids (HNO_3, H_2SO_4, lactic acid) resulted in the formation of various different nanostructures. The addition of NH_4F to the acidic electrolytes accelerated the growth rate resulting in bismuth-based nanostructures with comparably smaller dimensions and an enormous volume expansion observed during the growth. On the other hand, the addition of lactic acid to the acidic electrolytes decelerated the oxide growth rate. The resulting nanostructures were characterized using SEM, XRD and TEM. BiOCl nanoplatelets received by anodization in 1 M HCl were successfully employed for the photocatalytic decomposition of methylene blue dye and showed a superior performance compared to commercially available BiOCl powder with a similar crystalline structure, confirming its potential as a visible light photocatalyst.

During the last 20 years the anodic oxidation of valve metals for the synthesis of various nanotubular and nanoporous structures has been extensively exploited. Depending on the anodization conditions (i.e. applied potential/current density and electrolyte), highly ordered and self-organized nanostructured oxide films can be received, as e.g. Al_2O_3 nanopores[1] and TiO_2 nanotubes.[2,3] Even though Al and Ti are by far the most investigated metals for anodization, also other valve metals, such as W,[4] Hf,[5] Nb,[6] Ta,[7] or Zr[8] and their alloys with Ti and Al[9–12] have been studied for the anodic formation of nanostructures due to the wide application possibilities of the resulting oxidic nanostructures. It must be pointed out that especially in case of Ti the optimal amount of fluoride ions in the anodization electrolyte plays an important role for the formation of self-organized TiO_2 nanotubular layers.[2,3] It is therefore very reasonable to evaluate the impact of fluoride ions also on less common metals, such as bismuth.

The anodization of Bi dates back to the 1930's.[13] Further investigations were carried out in the 1960's and 1970's.[14–16] However, significant efforts to anodize Bi to receive Bi_2O_3 nanostructures were just carried out within the last decade.[17–28] The first article on the formation of Bi-based nanostructures upon the anodization of Bi was published by Yang et al. in 2010.[17] The authors received $BiPO_4$ nanorods by anodization of Bi sheets in phosphoric acid containing various concentrations of HF, an electrolyte that was also used to produce TiO_2 nanotube layers.[29,30] Nanoporous Bi_2O_3 films were produced by anodization in glycol electrolyte containing $(NH_4)_2SO_4$ and H_2O,[18] as well as in citric acid based electrolytes.[19–22]

Ahila et al. reported on the anodization of Bi in diluted sodium hydroxide solution[23,24] to fabricate nanostructured Bi_2O_3 films. The same authors also described the anodization in diluted oxalic acid for the fabrication of seaweed like Bi_2O_3 nanostructures.[25,26] In all cases, crystalline Bi_2O_3 was received after annealing of the anodized structures. Recently, we reported on the preparation of Bi_2O_3 needles upon anodization of Bi ingots in H_2SO_4 and subsequent annealing.[27] Furthermore, Zhao et al.[28], described the fabrication of BiOX nanosheeted films by anodization in electrolytes containing NH_4Cl, HBr or NH_4I, respectively, and their application for the photocatalytic degradation of methyl orange. However, details on the electrochemical preparation, i.e. on the anodization under dielectric breakdown conditions, were not discussed in that study.[28]

Bi_2O_3, as well as BiOCl, gained large attention in the recent years due to their broad applications in photocatalysis[31,32] or sensors.[33,34] Bi_2O_3 can furthermore be used, for instance, in solid oxide fuel cells[35] or supercapacitors.[36] For these applications, nanostructures are of high interest owing to their large active surface area.

[a] Dr. H. Sopha, L. Hromadko, Dr. J. M. Macak
Center of Materials and Nanotechnologies
Faculty of Chemical Technology
University of Pardubice
Nam. Cs. Legii 565, 53002 Pardubice (Czech Republic).
E-mail: hannaingrid.sopha@upce.cz
jan.macak@upce.cz
[b] Dr. H. Sopha, Dr. Z. Spotz, J. Michalicka, Dr. J. M. Macak
Central European Institute of Technology
Brno University of Technology
Purkyňova 123, 612 00 Brno (Czech Republic).
[c] Prof. R. Bulanek
Department of Physical Chemistry
Faculty of Chemical Technology
University of Pardubice
Studentska 573, 53 210, Pardubice (Czech Republic).
[d] Prof. T. Wagner
Department of General and Inorganic Chemistry
Faculty of Chemical Technology
University of Pardubice
Studentska 573, 53 210, Pardubice (Czech Republic).

Supporting information for this article is available on the WWW under https://doi.org/10.1002/celc.201801280

In this publication, the preparation of BiOCl nanoplatelets upon Bi anodization under dielectric breakdown conditions in diluted HCl based electrolytes is presented. Furthermore, the anodization of Bi in other common inorganic acids (i.e. H_2SO_4 and HNO_3), typically used for corrosion studies, is shown. Last, but not least, also lactic acid was chosen as an electrolyte and electrolyte additive, as it is (to a certain extent) used as an additive to electrolytes employed for the anodization of Ti.[37] In contrast to the previously mentioned report by Zhao et al.,[28] this work is focussed on the specific features of a dielectric breakdown of Bi, namely breaking of its passivity and its very rapid oxidation in the presence of acids accompanied by enormous pitting and consumption of Bi. Moreover, the influence of electrolyte additives, such as NH_4F, or lactic acid, on the anodization (the current density-time plots and on the received nanostructures) is thoroughly discussed. The resulting structures were annealed at 200 °C and investigated using scanning electron microscopy (SEM) and X-ray diffraction (XRD). Additionally, extensive transmission electron microscope (TEM) analyses were carried out. The applicability of BiOCl platelets prepared in HCl was shown for photocatalytical degradation of a model dye - methylene blue (MB).

Figure 1 shows SEM images of the structures received after the breakdown anodization of Bi ingots at 20 V for 30 min in three different electrolytes: 1 M HCl, 1 M HCl mixed with 0.1 M NH_4F, and 1 M HCl mixed with 70% lactic acid (LA). As can be seen, nanoplatelets of different sizes were grown in the different electrolytes. In pure HCl, the nanoplatelets had a diameter of ~120–130 nm and a height of ~25–30 nm, while in HCl mixed with NH_4F the nanoplatelets had a thickness of ~16 nm (the diameter was not measureable from the SEM images due to the order of the platelets). In HCl mixed with LA, nanoplatelets with a diameter between ~100 and ~200 nm and a thickness of ~25–30 nm were received.

During the anodization experiments in HCl or HCl mixed with NH_4F, a huge volume expansion was observed resulting in very bulky layers with poor adhesion to the Bi substrate, with a somewhat greater volume expansion observed in the mixed electrolyte than in the pure HCl. In contrast, when the electrolyte consisted of HCl mixed with LA, the volume expansion was rather insignificant, resulting in a thin white layer obtained on the surface of the anodized Bi ingot.

The addition of NH_4F and LA to the electrolyte has straight forward reasons: i) the presence of F^- ions is required for the fabrication of TiO_2 nanotube layers,[2] thus, the effect of their presence on the anodization of Bi should be studied as well, ii) it is known from the literature for nanotubular TiO_2 layers that if LA is added to the electrolyte, the anodization potential can be increased without the risk of breakdown.[37]

The reference anodization of Bi in aqueous 0.1 M NH_4F electrolyte (i.e. without the addition of HCl) resulted in the formation of sponge-like, bulky layer on the ingot (Figure S1). It should be mentioned that NH_4F concentrations ~0.1 M–0.2 M NH_4F are typical for the anodization of Ti that yield in the formation of TiO_2 nanotubular layers. Preliminary experiments adding higher concentrations of NH_4F to the electrolyte for Bi anodization did not show any promising nanostructures, for lower concentrations no remarkable differences were obtained compared to 1 M HCl. In none of the cases (i.e. HCl with any concentration of NH_4F), structures similar to TiO_2 nanotubular layers were formed, which points out on the fact that different valve metals have different prerequisites for the growth of self-organized structures.

The use of aqueous 70% LA as anodization electrolyte lead to an etching of the surface of the Bi ingot into a branched microstructure, macroscopically possessing the colour of metallic Bi and yielding a shallow crater in the ingot after the anodization (Figure S2).

Figure 2 shows the polarization curves and current density vs time plots for the anodization of Bi in HCl based electrolytes corresponding to Figure 1. Very high current densities were recorded in HCl and HCl mixed with NH_4F, while the current density recorded in HCl mixed with LA was comparably low. In any case, the current densities for the anodization in these

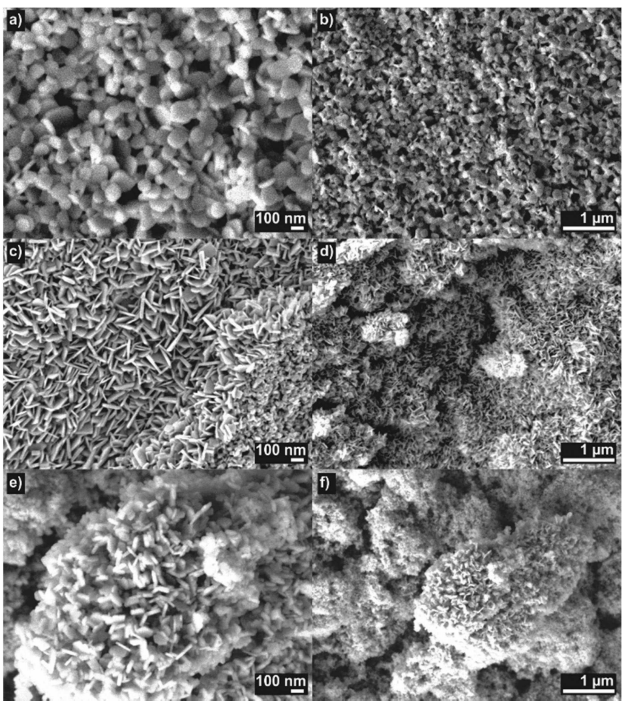

Figure 1. SEM images of Bi nanostructures received upon anodization at 20 V (sweep: 10 V/s) for 30 min in a), b) 1 M HCl, c), d) 1 M HCl + 0.1 M NH_4F, e), f) 1 M HCl + 70% LA.

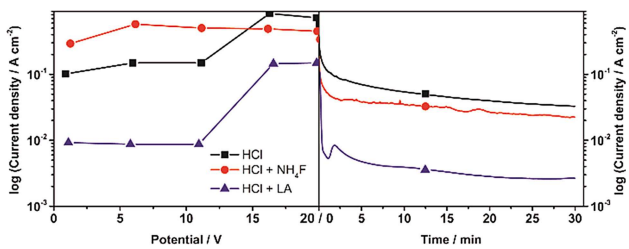

Figure 2. Polarization curves (left) and current-time plots (right) for the anodization of Bi in 1 M HCl, 1 M HCl + 0.1 M NH_4F and 1 M HCl + 70% LA at 20 V for 30 min (sweep:10 V/s).

three electrolytes increased strongly during the sweeping of the potential. The formation of the nanostructures was initiated due to breakdown of the Bi passivity and its fast oxidation. Afterwards, when 20 V were reached, the current densities were constant for a few seconds. Then the current densities decreased in time, but by far did not reach the level of dozens or hundreds of $\mu A\,cm^{-2}$, which is common for passive oxide films on metals. It is evident that the breakdown anodization presented here is accompanied by huge current densities, as in the case of breakdown anodizations of Ti and W.[38] Another similar feature is that shorter anodization times are required to obtain a huge volume of resulting material compared to classical anodization, where much longer anodization times are required. Thus, the presented synthesis is very efficient in terms of the quantity of material produced.

It should be mentioned that the anodization potential (20 V), the potential sweep rate (10 V/s) and the anodization time (30 min) were chosen based on preliminary experiments. The voltage and sweep rate were found to be sufficient to initialize the breakdown conditions, while the used anodization time was sufficient to produce substantial amounts of materials for analyses and photocatalytic testing. However, identical structures as shown in Figure 1 would be produced also if shorter times (e.g. 1 min) were used but in lower quantity.

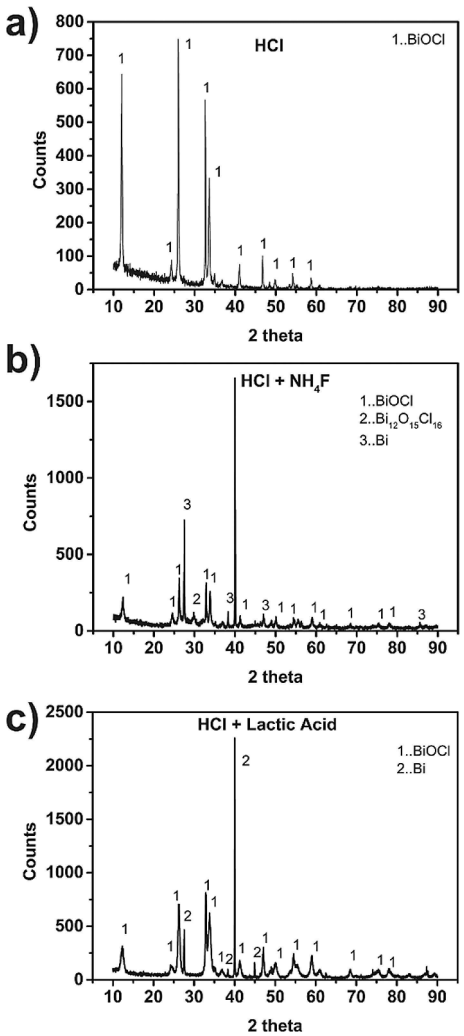

Figure 3. XRD patterns of the nanoplatelets received by anodization of Bi in a) 1 M HCl, b) 1 M HCl + NH_4F, and c) 1 M HCl + 70 % LA after annealing at 200 °C.

One can see that the addition of NH_4F to the electrolyte caused an increase of the current density at the beginning of the anodization and, thus, accelerated the reaction kinetics and the oxide growth towards greater volume expansion. This is also in agreement with the SEM observations. The Bi oxidation rate was higher during the anodization and, thus, thinner nanoplatelets were formed as they had shorter time to grow compared to NH_4F-free HCl (i.e. there was a shorter contact time of the electrolyte with the particular Bi species at the anodization interface during their oxidation).

In case of the addition of LA to the electrolyte the opposite effect to NH_4F addition was observed: the anodization reaction was decelerated, the oxide growth rate was smaller. The volume expansion of the oxide during anodization was comparably lower than during anodization in pure HCl and a relatively low current density was obtained. As already mentioned earlier, it is known from the literature for nanotubular TiO_2 layers that if LA is added to the electrolyte, the anodization potential can be increased without the risk of breakdown.[37] In other words, the addition of LA to the electrolyte increases the breakdown potential significantly. Herein, the potential was kept intentionally the same as for the other anodizations (20 V) for the purpose of comparison. As a result, the oxide growth rate was significantly decelerated.

It must be noted that the same phenomenon was observed when other common acids (i.e. H_2SO_4 and HNO_3) and their mixtures with NH_4F and LA were used as electrolyte for the anodization of Bi. However, the resulting nanostructures possess different shape than upon anodization in HCl (Figures S2 and S3).

To gain knowledge about the crystallinity of the received Bi nanostructures, XRD measurements were carried out, as shown in Figure 3 for the nanoplatelets obtained in HCl based electrolytes. The as-anodized structures showed already well-crystalline BiOCl. XRD patterns for H_2SO_4 and HNO_3 based electrolytes are shown in Figure S4. The as-anodized structures obtained in HNO_3 based electrolytes were crystalline, however, consisted of some non-stoichometric oxy-nitrates. The as-anodized structures obtained in H_2SO_4 based electrolytes showed only amorphous structure. This shows that at the given thermodynamic situation, the structures produced in HCl and HNO_3 had time to crystallize. However, all nanostructures were annealed directly on the Bi ingots at 200 °C for 2 hours to keep the treatment under the same conditions. This relatively low annealing temperature was employed because of the low melting point of Bi (~271 °C). When higher annealing temperatures were used, e.g. 250 °C, the underlying ingots got soft and started to change their shape.

A well crystalline BiOCl (74502-ICSD) structure was received upon anodization of Bi in all used HCl based electrolytes and subsequent annealing. In the mixture of HCl and NH_4F additionally some non-stoichometric $Bi_{12}O_{15}Cl_{16}$ (602-ICSD) was received. The signal of Bi that was seen for the nanoplatelets obtained

upon anodization in mixtures of HCl with NH_4F and LA, respectively, can be ascribed to the underlying Bi substrate from which the nanoplatelets grew.

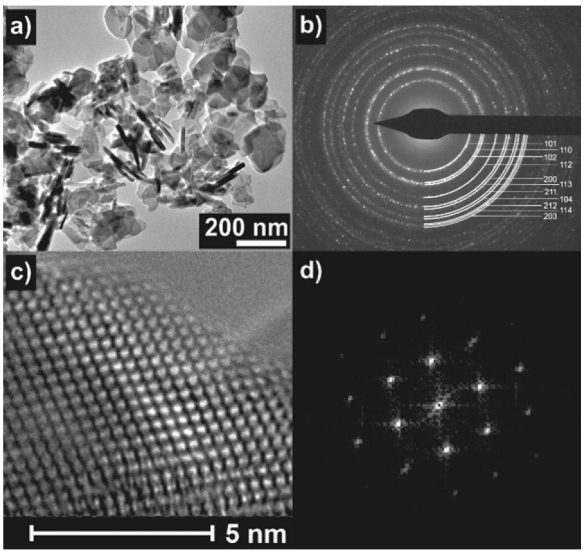

Figure 4. a) TEM image of the BiOCl nanoplatelets received upon anodization in 1 M HCl and annealing at 200 °C, b) SAED pattern of the nanoplatelets shown in a) with indicated crystallographic planes (evaluated from d-spacings), c) HR-TEM image of a single BiOCl nanoplatelet, d) FFT pattern of the nanoplatelet shown in (c).

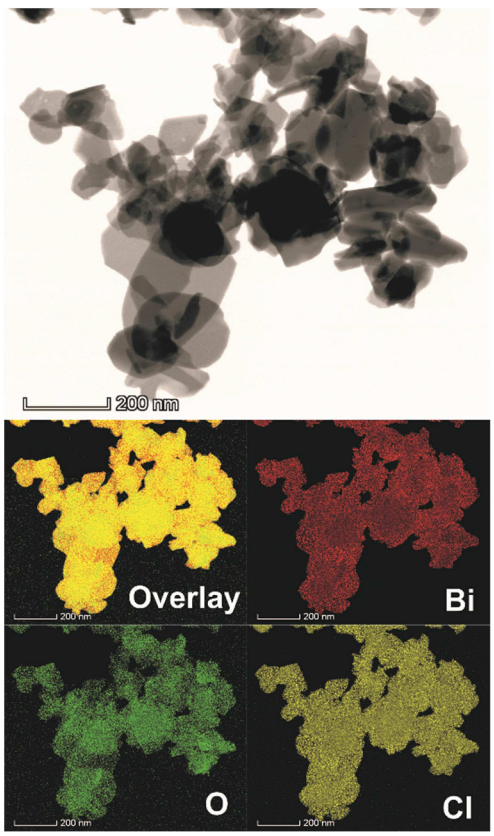

Figure 5. STEM image of the BiOCl nanoplatelets received upon anodization in 1 M HCl and annealing at 200 °C and the corresponding STEM/EDX elemental maps.

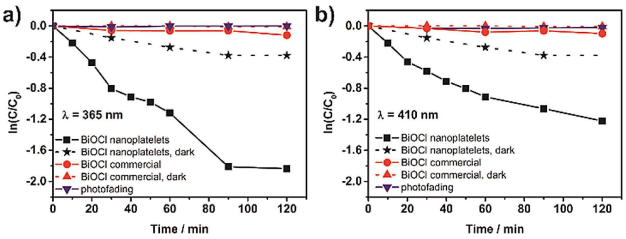

Figure 6. Photocatalytic decomposition of MB at a) λ = 365 nm, and b) λ = 410 nm, using BiOCl nanoplatelets and commercial BiOCl.

Thus, in general the following reaction for acidic Cl^- containing electrolytes [Eq. (1)] is suggested:

$$Bi + Cl^- + H_2O \xrightarrow{\Delta U,\ H^+} BiOCl + 2\,H^+ + 3\,e^- \quad (1)$$

TEM investigations were carried out for the nanoplatelets obtained from two electrolytes: HCl and HCl mixed with NH_4F. Figure 4a shows TEM images of the BiOCl nanoplatelets received upon anodization in 1 M HCl. Figure 4b depicts the corresponding selected area electron diffraction pattern (SAED). As can be seen, different crystallographic BiOCl planes were observed for the nanoplatelets. A high resolution TEM image of the nanoplatelets is shown in Figure 4c with the corresponding FFT pattern in Figure 4d. From this image it is clearly visible that the visualized nanoplatelet is single-crystalline. Thus, it might be suggested that the BiOCl nanoplatelets received in HCl are single-crystalline, but the different platelets differ in the orientations of the crystallographic planes resulting in the SAED pattern shown in Figure 4b, when measured over several nanoplatelets.

Figure 5 shows a STEM image and the corresponding STEM/EDX elemental maps of the nanoplatelets received upon anodization in HCl and subsequent annealing at 200 °C. A homogenous distribution of Bi, O and Cl was observed, proving that BiOCl of a good quality and purity was received.

Figure S5 depicts the STEM image of BiOCl nanoplatelets produced via anodization in 1 M HCl + 0.1 M NH_4F and annealing at 200 °C. As can be seen, the nanoplatelets were smaller than the nanoplatelets received upon anodization in pure HCl. This is in agreement with the previously discussed results shown in Figures 1 and 2: the oxide growth was accelerated when NH_4F was added to the electrolyte. As a result, the nanoplatelets were smaller in their overall size.

Since BiOCl was shown to be a good photocatalyst,[31,39] the photocatalytic performance of the nanoplatelets obtained in HCl was investigated for the decomposition of methylene blue (MB) as a model dye.[40] These nanoplatelets were tested against a commercially available BiOCl powder as reference photocatalyst. Two different wavelengths in the UV and in the VIS light, i.e. 365 nm and 410 nm, were employed. The results are shown in Figure 6. Under both illumination wavelengths, the BiOCl nanoplatelets revealed significantly higher decomposition rates than the commercial BiOCl powder. For the BiOCl nanoplatelets, rate constants of 1.923×10^{-2} min^{-1} (first 90 min) and 1.485×10^{-2} min^{-1} (first 60 min) were obtained for irradiation at

a wavelength of 365 nm and 410 nm, respectively. For the commercial BiOCl powder, the rate constants were 8.017×10^{-4} min^{-1} for an irradiation at 365 nm and 7.540×10^{-4} min^{-1} for an irradiation at 410 nm. To find reasons for these results the specific surface areas of the BiOCl nanoplatelets and the commercial BiOCl powder were determined from N_2 adsorption isotherms using BET method. The specific surface areas were calculated to 8.9 m^2/g and 1.2 m^2/g for the nanoplatelets and the commercial powder, respectively (see Figure S6). Thus, the surface area of the BiOCl nanoplatelets obtained by anodization is approximately 7.5 times as high as the surface area of the commercial BiOCl powder. A SEM image of the commercial BiOCl powder is shown in Figure S7. It can be seen that the particle size is much larger with an average diameter of ~1 μm compared to the BiOCl nanoplatelets shown in Figure 1 (diameter 120–130 nm, thickness 25–30 nm). Additionally, the crystallinity of the BiOCl nanoplatelets and the commercial BiOCl powder were investigated using XRD (Figure S8). As can be seen, the crystallinity of both compounds was very similar. Thus, it can be assumed that the higher surface area of the well crystalline BiOCl nanoplatelets was the main factor leading to the significantly higher decomposition rates of MB.

In summary, it was shown that the dielectric breakdown anodization of Bi ingots at 20 V in electrolytes consisting of either HCl or mixtures of HCl with NH_4F and or LA results in the formation of nanoplatelets of different dimensions. By anodization under the same conditions in other common acids a variety of different Bi based nanostructures can be received. The anodization experiments in this work were carried out intentionally under dielectric breakdown conditions, otherwise the growth of nanostructured oxides would not take place. By adding NH_4F to the electrolyte the oxide growth rate was accelerated, while the addition of LA was decelerated the oxide growth rate. XRD measurements showed that the received nanostructures consisted of BiOCl after annealing at 200 °C for HCl based electrolytes. The BiOCl nanoplatelets received upon anodization in HCl showed a superior photocatalytic behaviour in the UV light as well as in the VIS light, compared to commercial BiOCl powder. The presented results clearly show that anodization of Bi is a very simple and practical technique for the synthesis of various Bi based nanostructures with interesting properties. These materials will surely be exploited in future for various applications in catalysis, sensing and thermoelectrics.

Experimental Section

A Bi rod (purity 99.9995 %, Unterharzer Berg- und Hüttenwerke GmbH, Goslar) was cut into ingots of 1.5×1.5 cm^2 with a thickness of ca. 5 mm. Before anodization the ingots were degreased by sonication in isopropanol. The anodizations were carried out in various electrolytes, applying a potential of 20 V for 30 min at a temperature of 5 °C with a sweep rate of 10 V/s. The electrolytes consisted of 1 M HCl (Penta Chemicals), 1 M H_2SO_4 (Penta Chemicals), 1 M HNO_3 (Penta Chemicals), 70 % lactic acid (~9.3 M) (Sigma-Aldrich), 0.1 M NH_4F (Sigma-Aldrich) and mixtures of these solutions.

The electrochemical cell consisted of a high-voltage potentiostat (PGU-200 V, Elektroniklabor GmbH) in a two-electrode configuration, with a Pt foil as counter electrode and a Bi substrate as working electrode, pressed against an O-ring of the electrochemical cell, leaving 0.071 cm^2 or 1 cm^2 open to the electrolyte. After anodization the anodized layers were carefully rinsed with DI water and dried in air. Annealing of the anodized Bi ingots was carried out in a muffle oven at 200 °C for 2 h in air.

The structure and morphology of the anodized layers were characterized by a scanning electron microscope (SEM, JEOL JSM 7500F) and a scanning transmission electron microscope (HR-TEM FEI TITAN Themis 60–300 with X-FEG type emission gun) equipped with Cs image corrector and a STEM high-angle annular dark-field detector (HAADF). The point resolution was 0.06 nm in TEM mode. The elemental mappings were obtained by STEM-Energy Dispersive X-ray (EDX) spectroscopy using FEI SUPER-X windowless detector and an acquisition time of about 20 min. X-ray diffraction analyses (XRD) were carried out in the micro-diffraction mode with an X-ray diffractometer (Rigaku SmartLab 3 kW) using Cu Kα radiation.

In order to determine specific surface area, N_2 adsorption/desorption isotherms were measured on samples degased at 200 °C for 8 h under dynamic turbomolecular pump vacuum. The isotherms were acquired using an ASAP 2020 instrument (Micromeritics) and evaluated by MicroActive software (Micromeritics). The specific surface area was calculated according to the BET method.[41]

For photocatalytic test, 10 ml 1×10^{-5} M methylene blue (MB) solution were mixed with 10 mg BiOCl nanoplatelets or 10 mg commercial BiOCl powder (Sigma-Aldrich) as catalyst. The mixtures were stirred for one hour in the dark to reach the dye adsorption-desorption equilibrium. Then, the solutions were irradiated by a LED-based UV lamp (power output = 10 W, wavelength = 365 nm ± 5 nm) or by a LED-based VIS lamp (power output = 10 W, wavelength = 410 nm ± 5 nm) and the absorbance of the MB solution was periodically measured (10 min or 30 min steps) by a UV–VIS spectrometer (S-200, Boeco) at a wavelength of 670 nm to monitor the decomposition rates. For comparison, some experiments were also conducted in the dark.

Acknowledgements

Ministry of Youth, Education and Sports of the Czech Republic (projects nr. LM2015082, LM2015041, LQ1601, CZ.02.1.01/0.0/0.0/16_013/0001829) is acknowledged for financial support of this work.

Conflict of Interest

The authors declare no conflict of interest.

Keywords: anodization · bismuth · bismuth oxychloride · nanoplatelets · photocatalysis

[1] H. Masuda, K. Fukuda, *Science* **1995**, *268*, 1466–1468.
[2] J. M. Macak, H. Tsuchiya, A. Ghicov, K. Yasuda, R. Hahn, S. Bauer, P. Schmuki, *Curr. Opin. Solid State Mater. Sci.* **2007**, *11*, 3–18.
[3] K. Lee, A. Mazare, P. Schmuki, *Chem. Rev.* **2014**, *114*, 9385–9454.
[4] H. Tsuchiya, J. M. Macak, I. Sieber, L. Taveira, A. Ghicov, K. Sirotna, P. Schmuki, *Electrochem. Commun.* **2005**, *7*, 295–298.

[5] H. Tsuchiya, P. Schmuki, *Electrochem. Commun.* **2005**, *7*, 49–52.
[6] I. Sieber, H. Hildebrand, A. Friedrich, P. Schmuki, *Electrochem. Commun.* **2005**, *7*, 97–100.
[7] W. Wei, J. M. Macak, P. Schmuki, *Electrochem. Commun.* **2008**, *10*, 428–432.
[8] S. Berger, J. Faltenbacher, S. Bauer, P. Schmuki, *Phys. Status Solidi* **2008**, *2*, 102–104.
[9] H. Tsuchiya, J. M. Macak, A. Ghicov, P. Schmuki, *Small* **2006**, *2*, 888–891.
[10] H. Tsuchiya, S. Berger, J. M. Macak, A. Ghicov, P. Schmuki, *Electrochem. Commun.* **2007**, *9*, 2397–2402.
[11] J. M. Macak, H. Tsuchiya, L. Taveira, A. Ghicov, P. Schmuki, *J. Biomed. Mater. Res. Part A* **2005**, *75*, 928–933.
[12] H. Sopha, D. Pohl, C. Damm, L. Hromadko, B. Rellinghaus, A. Gebert, J. M. Macak, *Mater. Sci. Eng. C* **2017**, *70*, 258–263.
[13] A. Güntherschulze, H. Betz, *Z. Elektrochem.* **1931**, *37*, 726–734.
[14] L. Masing, L. Young, *Can. J. Chem.* **1962**, *40*, 903–920.
[15] I. A. Ammar, M. W. Khalil , *Electrochim. Acta* **1971**, *16*, 1601–1612.
[16] I. A. Ammar, M. W. Khalil , *J. Electroanal. Chem.* **1971**, *32*, 373–386.
[17] M. Yang, N. K. Shrestha, R. Hahn, P. Schmuki, *Electrochem. Solid-State Lett.* **2010**, *13*, C5-C8.
[18] X. Lv, J. Zhao, X. Wang, X. Xu, L. Bai, B. Wang, *J. Solid State Electrochem.* **2013**, *17*, 1215–1219.
[19] K. C. Chitrada, K. S. Raja, *ECS Trans.* **2014**, *61*, 1–12.
[20] K. C. Chitrada, K. S. Raja, R. Gakhar, D. Chidambaram, *J. Electrochem. Soc.* **2015**, *162*, H380-H391.
[21] K. C. Chitrada, R. Gakhar, D. Chidambaram, E. Aston, K. S. Raja, *J. Electrochem. Soc.* **2016**, *163*, H544-H558.
[22] M. Ahila, J. Dhanalakshmi, J. Celina Selvakumari, D. Pathinettam Padiyan, *Mater. Res. Express* **2016**, *3*, 105025.
[23] M. Ahila, M. Malligavathy, E. Subramanian, D. Pathinettam Padiyan, *Solid State Ionics* **2016**, *298*, 23–34.
[24] M. Ahila, M. Malligavathy, E. Subramanian, D. Pathinettam Padiyan, *Part. Sci. Technol.* **2018**, *36*, 655–569.
[25] M. Ahila, E. Subramanian, D. Pathinettam Padiyan, *Ionics* **2017**, *24*, 1827–1839.
[26] M. Ahila, E. Subramanian, D. Pathinettam Padiyan, *J. Electroanal. Chem.* **2017**, *805*, 146–158.
[27] H. Sopha, V. Podzemna, L. Hromadko, J. M. Macak, *Electrochem. Commun.* **2017**, *84*, 6–9.
[28] J. Zhao, X. Lv, X. Wang, J. Yang, X. Yang, X. Lu, *Mater. Lett.* **2015**, *158*, 40–44.
[29] A. Ghicov, H. Tsuchiya, J. M. Macak, P. Schmuki, *Electrochem. Commun.* **2005**, *7*, 505–509.
[30] K. S. Raja, M. Misra, K. Paramguru, *Electrochim. Acta* **2005**, *51*, 154–165.
[31] H. Weidong, Q. Wei, W. Xiaohong, D. Xianbo, C. Long, J. Zhaohua, *Thin Solid Films* **2007**, *515*, 5362–5365.
[32] X. Zhang, Z. Ai, F. Jia, L. Zhang, *J. Phys. Chem. C* **2008**, *112*, 747–753.
[33] A. Cabot, A. Marsal, J. Arbiol, J. R. Morante, *Sens. Actuators B* **2004**, *99*, 74–89.
[34] C. R. Michel, N. L. López Contreras, A. H. Martínez-Preciado, *Sens. Actuators B* **2011**, *160*, 271–277.
[35] A. M. Azad, S. Larose, S. A. Akbar, *J. Mater. Sci.* **1994**, *29*, 4135–4151.
[36] T. P. Gujar, V. R. Shinde, C. D. Lokhande, S.-H. Han, *J. Power Sources* **2006**, *161*, 1479–1485.
[37] S. So, K. Lee, P. Schmuki, *J. Am. Chem. Soc.* **2012**, *134*, 11316–11318.
[38] R. Hahn, J. M. Macak, P. Schmuki, *Electrochem. Commun.* **2007**, *9*, 947–952.
[39] F. Chen, H. Liu, S. Bagwasi, X. Shen, J. Zhang, *J. Photochem. Photobiol. A* **2010**, *215*, 76–80.
[40] B. Sarwan, B. Pare, A. D. Acharya, *Mater. Sci. Semicond. Process.* **2014**, *25*, 89–97.
[41] S. Brunauer, P. H. Emmet, E. Teller, *J. Am. Chem. Soc.* **1938**, *60*, 309–319.

Manuscript received: September 13, 2018
Accepted manuscript online: October 8, 2018
Version of record online: October 31, 2018